Seismic imaging beneath Sumatra Island and its surroundings, Indonesia, from local-regional P-wave earthquake tomography

Bayu Pranata[1], Mohamad Ramdhan[2], Muhammad Hanif[2], Muhammad Iqbal Sulaiman[3], Mufti Putra Maulana[4], Wandono[4], Sri Widiyantoro[5], Sandy Kurniawan Suhardja[6], Edi Hidayat[2], Pepen Supendi[1], Ridwan Kusnandar[1], Wiko Setyonegoro[2]

[1] Indonesian Agency for Meteorology, Climatology, and Geophysics (BMKG), Jalan Angkasa I, No. 2, Kemayoran, Jakarta 10720, Indonesia

[2] Research Center for Geological Disaster, National Research and Innovation Agency (BRIN), KST Samaun Samadikun, Jl. Cisitu Sangkuriang, Bandung 40135, Indonesia

[3] Luwu Disaster Management Agency (BPBD Kab. Luwu), Jl. Andi Djemma, Senga, Belopa, Kab. Luwu 91994, Indonesia

[4] School of Meteorology, Climatology, and Geophysics of Indonesia (STMKG), Jl. Perhubungan I No. 5, Pondok Betung, Tangerang Selatan 15221, Indonesia

[5] Global Geophysics Research Group, Faculty of Mining and Petroleum Engineering, Institut Teknologi Bandung, Bandung 40132, Indonesia; Faculty of Engineering, Maranatha Christian University, Bandung 40164, Indonesia

[6] University of Pertamina, Jl. Teuku Nyak Arief, Simprug, Kebayoran Lama, Jakarta 12220, Indonesia

Abstract

Sumatra Island and its surroundings, Indonesia, are one of the most active tectonics in the world. The Aceh-Andaman earthquake, one of the most destructive earthquakes in the world, occurred there. It has attracted many earth scientists to apply various methods, including seismic tomography, to understand the island's subsurface structure and tectonic system. This study is the first to delineate subsurface imaging beneath the island and its surroundings using a local-regional earthquake catalogue from the Indonesian Agency for Meteorology, Climatology, and Geophysics (BMKG) seismic network. The tomographic imaging of P-wave (Vp) conducted in this study has successfully delineated subduction slabs (high Vp), partial melting zones (low Vp), volcanic arcs (low Vp), and Sumatran Fault zones (low Vp). The relationship between the subduction zone and the volcanic arc on the island can be seen on several vertical sections where a partial melting zone occurs at a depth of about 100 km, which functions as magma feeding for some volcanoes on the island. The oceanic slab model also exhibits a more pronounced and steeper slope towards the southern regions of Sumatra Island, possibly attributed to the slab's aging process in that direction. The results highlight the importance of the BMKG seismic network in imaging local-regional subsurface structures beneath Indonesia's archipelago, especially for the main islands such as Sumatra.

Keywords:
Sumatra; BMKG, P– wave; tomography; slab; fault

1. Introduction

Sumatra Island and its surroundings are among the areas in Indonesia with very high seismic activity. Seismic activity in this region is caused by the oblique subduction of the Australian Plate to the Southeast Asian Plate. The offshore plate boundary of Sumatra Island, Indonesia, is formed due to the oblique subduction of the Indian and Australian sub-plates beneath the Sunda Plate at variable rates of 5-6 cm/year (**DeMets et al., 2010**). Subduction resulted in two central tectonic systems: the subduction zone fault system along the Sumatra Sea trench and the Sumatran Fault System. The second fault system, known as the Sumatran Fault, is a strike-slip fault with a dextral direction that spans the 1900 km Sumatran backbone, consisting of 20 main segments and is located close to the volcanic arc of the island of Sumatra (**Irsyam et al., 2017**; **Natawidjaja, 2018**; **Sieh & Natawidjaja, 2000**). The Sumatran Fault Zone (SFZ) spans from the Sunda Strait in the south with a tectonic strain rate of ±6 mm/year to the Andaman Sea in the north with a rifting rate of 37 mm/year, while exhibiting varying slip rates, such as ~9 mm/year in the Sunda Strait and on the Kumering Fault in south Sumatra, 14-15 mm/year near Lake Maninjau in central Sumatra, and 16±6 mm/year across the Batee and Takengon segments in the Aceh region, increasing to 20±6 mm/year across the Aceh segment (**Natawidjaja, 2018**). Oblique subduction plays a crucial role in forming the ±600 km Menta-
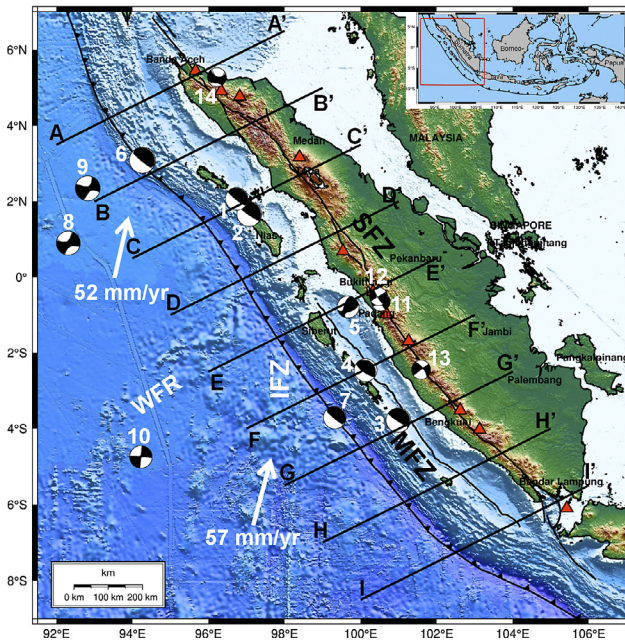
Figure 1: The main tectonic settings in the study area consist of the subduction zone, the Sumatran Fault Zone (SFZ), and the Mentawai Fault Zone (MFZ) (modified from Irsyam et al., 2017). In addition, Wharton Fossil Ridge (WFR) and Investigator Fracture Zone (IFZ) are two tectonic features found in the research area. The study area is in the red box in the inset figure. Earthquake events numbering follows the sequential chronological order. Based on the location, events 1 to 7 occurred on the subduction zone of Sumatra Island, events 11 to 14 occurred on the mainland of Sumatra Island or in the Sumatran Fault Zone (SFZ), and events 8 to 10 occurred in the WFR area. The plate movement rate is modified from Natawidjaja, 2018. The red triangle shows the volcano's position on Sumatra Island and its surroundings (modified from Malawani et al., 2021). The cross-sectional lines A-A' to I-I' are the vertical section of the tomogram directions that pass through Sumatra Island from north to south. The source mechanism shown on the map is modified from the CMT global catalogue (Ekström et al., 2012). The topographic map in the image above uses GEBCO data (modified from Weatherall et al., 2015).

wai fault system, which operates parallel to the Sumatran Fault System. This process contributes to the uplift of the accretionary wedge and the deposition of sediments in the forearc basin, resulting in the development of elongated Neogene basin depocenters aligned parallel to the trench in the Sumatran forearc region (**Mukti et al., 2021**). The Mentawai fault system is located in the fore-arc basin from the southernmost Sumatra to the north of Siberut Island, the Mentawai Islands. **Figure 1** shows the tectonic system of Sumatra Island and its surroundings, along with several significant earthquakes between 2004 and 2016, as shown in **Table 1**. Additionally, **Figure S1** displays the most recent segments of the Sumatran Fault System.

The heightened seismic activity in this region has sparked considerable interest among earth scientists aiming to comprehend the earthquake source character-

istics and their potential impact. Both aspects hold great value in mitigating earthquake disasters in the area. Various geophysical methods have been devised and employed to investigate these aspects. As these characteristics are influenced by processes occurring beneath the earth's surface, a comprehensive understanding of the subsurface structure becomes paramount. Seismic tomography serves as a primary method for comprehending the earth's subsurface structure on a local to a global scale, and it has been effectively utilized in the study of Sumatra Island and its surrounding areas. Local seismic tomographic studies in the Toba Caldera area have determined a magma reservoir 5 km below sea level characterized by a high Vp/Vs value of 1.9 (**Koulakov et al., 2009**). The study also described the partial melting zone that serves as the source of the caldera magma and the mantle wedge structure indicated by low Vp, and high Vp/Vs values. The subsurface structure was delineated from earthquakes recorded by the PASSCAL seismic network consisting of 40 seismic stations (**Fauzi et al., 1996; Masturyono et al., 2001**). The results of this study were an update on previous studies that described subsurface structures using only P– waves (**Masturyono et al., 2001**). Global seismic tomographic studies under the Burma, Andaman, and Sumatra arcs have detected the presence of slabs to a depth of 975 km beneath the island of Sumatra to the Andaman (**Pesicek et al., 2008**). This study has updated the previous global seismic tomography studies by adding new data and using different methods (**Widiyantoro & van der Hilst, 1996, 1997**). Teleseismic tomography has succeeded in depicting the subducted slab under the northern part of Sumatra Island to a depth of 400 km and the subduction of the slab in the southern part to 800 km (**Liu et al., 2018**). The study utilized the BMKG seismic network. Joint inversion using regional earthquake and teleseismic data with the same seismic networks has successfully described the morphology of the slab under northern Sumatra (**Liu et al., 2019**). An exciting feature of the study was the ability to explain the slab tear caused by the subduction of the IFZ under the Toba Caldera at a depth of 120 km to more than 400 km. The latest regional seismic tomography study using data from the International Seismological Centre (ISC) has determined the seismic velocity structure of P– waves to a depth of 90 km (**Osagie and Abir, 2021**).

This research focuses on analysing earthquakes in and around Sumatra, by utilizing data recorded on the local-regional seismic network operated by BMKG. The study presents updated tomographic findings of the P-wave seismic velocity (Vp) beneath Sumatra and its surrounding areas, using a more recent earthquake catalogue compared to previous studies. It is worth noting that the previous BMKG earthquake catalogue has yet to be employed for tomographic investigations in Sumatra. However, the study did not incorporate tomographic models of the S-wave seismic velocity (Vs). This deci-

Table 1: Earthquake events and corresponding information analysed in this study

Event No.	Magnitude	Date	Remarks	Reference
1	Mw ~ 9.2	December 2004	Aceh-Andaman megathrust earthquake in December 2004	**(Meltzner et al., 2006)**
2	Mw 8.6	March 2005	March 2005 Nias earthquake	**(Fujii et al., 2020)**
3	Mw 8.4	September 2007	Bengkulu earthquake in September 17, 2007	**(Ekström et al., 2012)**
4	Mw 7.9	September 2007	Aftershock of Bengkulu earthquake	**(Ekström et al., 2012)**
5	Mw 7.6	September 2009	Intraslab earthquake on the west coast of Sumatra	**(Earthquake Engineering Research Institute (EERI), 2009)**
6	Mw 7.8	April 2010	Earthquake near the Banyak islands on April 7, 2010	**(Haridhi et al., 2018)**
7	Mw 7.8	October 2010	Megathrust earthquake around Sumatra Island on October 25, 2010	**(Ekström et al., 2012)**
8	Mw 8.6	April 2012	Intraplate event near Wharton Fossil Ridge (WFR) zone on April 11, 2012	**(Ekström et al., 2012)**
9	Mw 8.2	April 2012	Intraplate event near Wharton Fossil Ridge (WFR) zone on April 11, 2012	**(Ekström et al., 2012)**
10	Mw 7.8	March 2016	Intraplate event near Wharton Fossil Ridge (WFR) zone on March 2, 2016	**(Ekström et al., 2012)**
11	Mw 6.4	March 2007	Doublet earthquake on the Sumatran Fault on March 6, 2007	**(Nakano et al., 2010)**
12	Mw 6.3	March 2007	Doublet earthquake on the Sumatran Fault on March 6, 2007	**(Nakano et al., 2010)**
13	Mw 6.6	October 2009	Dikit segment earthquake in Bengkulu Province on October 1, 2009	**(Ekström et al., 2012)**
14	Mw 6.5	December 2016	Pidie Jaya earthquake on December 6, 2016	**(Muzli et al., 2018)**

sion was attributed to the scarcity of S-wave arrival times in the earthquake catalogue compared to the abundance of P-wave arrivals. Consequently, developing S-wave tomograms based on the existing earthquake catalogue would result in unreliable interpretations owing to inadequate resolution. To overcome this challenge, future seismic tomography studies that incorporate S-waves should prioritize identifying and re-picking wave phases. This process ensures that the time intervals between the two wave phases are not excessively distant, as observed in the existing earthquake catalogue.

2. Data and Methods

This study uses the BMKG earthquake catalogue for April 2009–December 2019 at coordinates 91.9º–108.2º east longitude and 7.5º south–6.9º north latitude or in Sumatra Island and its surroundings. The data used for tomographic inversion is a catalogue that has relocated its hypocentre parameters (**Ramdhan et al., 2021**). Every earthquake event was recorded by at least six stations so that seismic stations would accurately constrain the event's epicentre. The data used in this study is from 9,152 events recorded by 122 seismic stations on the island of Sumatra and its surroundings. **Figure 2** repre-
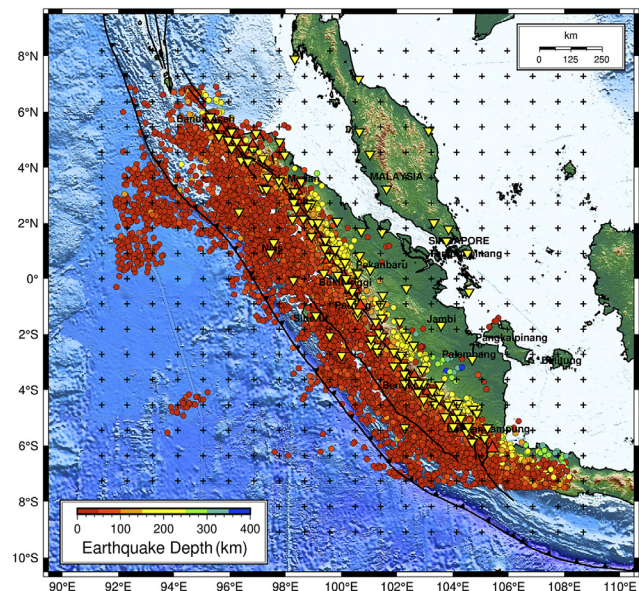
Figure 2: Grid configuration and hypocentre distribution used for seismic tomographic inversion. The inverted yellow triangle shows the seismic network that records the earthquakes.

sents earthquakes the BMKG seismic network recorded, and the grid distribution used for seismic tomographic inversion.

As depicted in **Figure 3**, the general process of tomographic inversion involves the utilization of an initial model $\mathbf{m}_0$ consisting of *Vp*, *Vp/Vs* ratios, and hypocentre parameters. This study incorporated a pre-existing 1-D velocity model with a *Vp/Vs* ratio of 1.73 (**Kennett et al., 1995**; **Wadati, 1933**). The hypocentre parameters were derived from the BMKG earthquake catalogue. The **Δd** matrix represents the discrepancy between observed travel times ($\mathbf{t}_{obs}$) and calculated travel times ($\mathbf{t}_{cal}$) of seismic waves at individual seismic stations. The calculation of $\mathbf{t}_{cal}$ is accomplished through forward modelling with the aid of **g(m)**. The matrix **J**, known as the Jacobian matrix, encompasses the first partial derivatives of the calculated travel times with respect to velocity parameters (*Vp* and *Vp/Vs*) and hypocentre parameters. The **Δm** matrix denotes the model perturbation matrix for velocity and hypocentre parameters, facilitating the iterative refinement of previous model parameters

until the minimum error criterion is met, thus signifying the attainment of the final model parameters (**m**).

The SIMULPS12 code was employed for inversion tomography, applying simultaneous inversion of the velocity model parameters (*Vp*) and the *Vp/Vs* ratio, along with the determination of hypocentres (**Evans et al., 1994**; **Thurber, 1993**). The pseudo-bending method was determined by ray tracing in the code (**Um & Thurber, 1987**). The algorithm has been successfully applied in various parts of Indonesia to determine subsurface structures and physical properties at different scales (**Afif et al., 2021**; **Ramdhan et al., 2019**; **Supendi et al., 2020**). The initial velocity model used for the inversion tomographic input applied the 1D AK135 model (**Kennett et al., 1995**). A uniform grid size of 100 km was used for the horizontal grid model. **Table 2** reveals a varying grid size ranging from 10 km to 50 km for the vertical grid distance. Damping determination is crucial for determining the optimal value during the tomographic inversion process. This value was derived from the trade-off curve depicted in **Figure 4**, which compared the data with the variance model. A damping value 70 was obtained from the first iteration of the tomographic inversion.

Prior to conducting tomographic inversion, it was crucial to perform resolution tests to assess areas or features that can be effectively resolved using seismic data. This study implemented a checkerboard resolution test (CRT), incorporating positive and negative perturbations of ±5% relative to the 1-D reference velocity model, which served as input for the tests. If the inversion results of the synthetic model exhibit similar patterns of negative or positive anomalies resembling the input perturbations, it could be inferred that those areas were successfully resolved by the seismic data, even with some magnitude reductions due to damping, which is a limitation of the resolution test (**Lévěque et al., 1993**; **Ramdhan et al., 2019**; **Rawlinson & Spakman, 2016**). This study only used a P– wave tomogram, so it was not too deep to discuss the physical properties of the rock, which required a tomogram of the *Vp/Vs* ratio, which was linear with Poisson's ratio. These parameters were susceptible to changes in fluid and temperature.
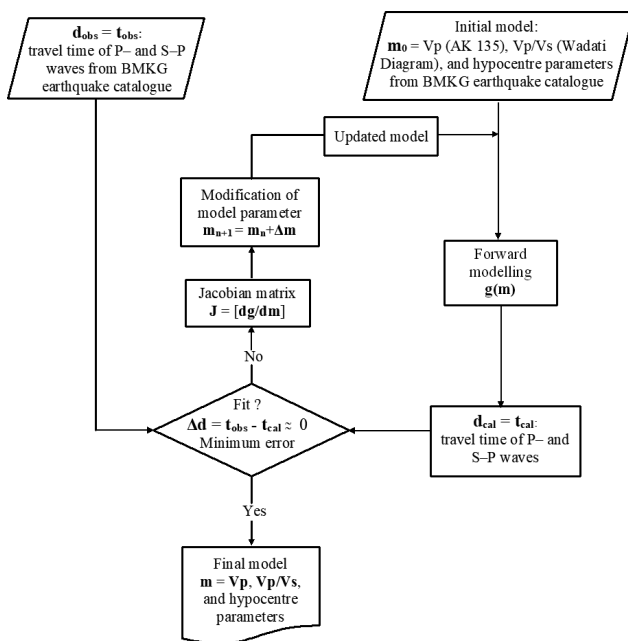
Figure 3: The general inversion algorithm for simultaneous inversion determination conducted in this study (modified from **Grandis, 2009**).

Table 2: The three-dimensional grid spacing in the horizontal (X and Y) and vertical (Z) directions, along with their corresponding distances from the center of grid utilized to delineate the seismic velocity structure beneath Sumatra Island and its surroundings.

Grid direction	Number of grid	Grid distances from the center of grid (km); Center of grid is at 100.5°E and 0.0°S									
X	20	-1000	-900	-800	-700	-600	-500	-400	-300	-200	-100
		0	100	200	300	400	500	600	700	800	900
Y	20	-1000	-900	-800	-700	-600	-500	-400	-300	-200	-100
		0	100	200	300	400	500	600	700	800	900
Z	18	-10	0	10	20	30	40	50	60	80	100
		120	150	180	200	250	300	350	400		
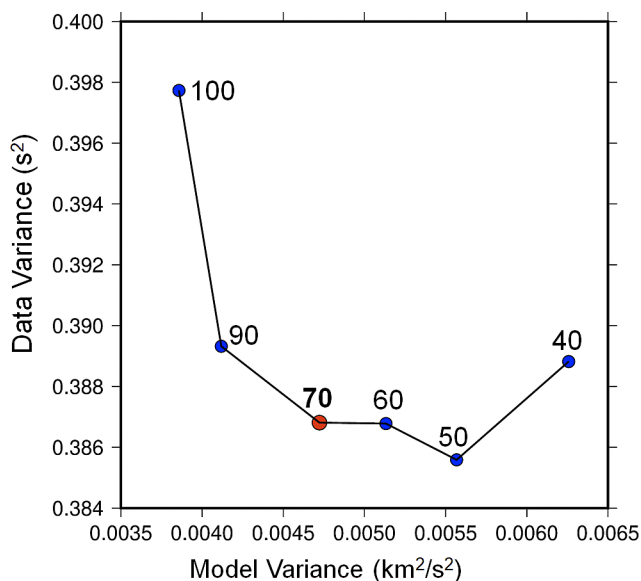
Figure 4: Trade-off curve to get optimum damping. The optimum damping value used is indicated by the red circle of 70. After one iteration of inversion, the values for various damping levels are represented by blue circles.

3. Results and Discussion

As mentioned above, this study used 9,152 events to image the subsurface structure beneath the research area. The total phases consist of 89,292 P-waves and 28,509 S-waves. The analysis of the tomographic inversion revealed promising results, as evidenced by the concentration of residual time ranging predominantly between -1 and 1 s, with a tendency towards approaching zero values (see **Figure 5**). However, despite focusing on P-wave analysis, this study incorporated S-phases in the simultaneous inversion process to provide additional
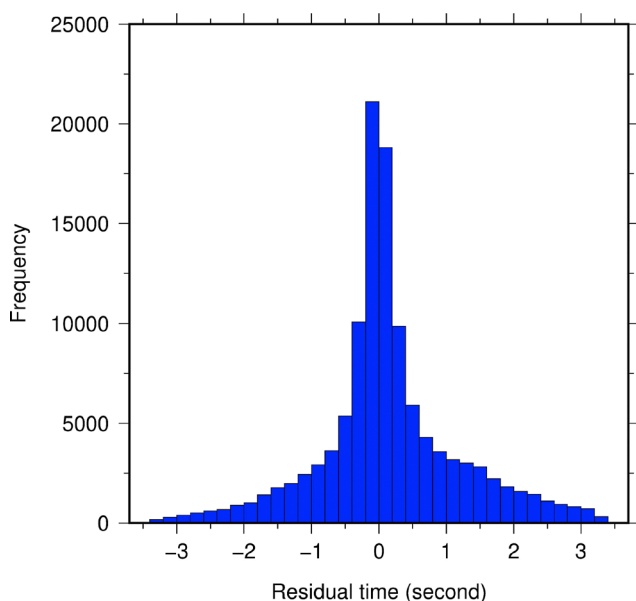
Figure 5: Residual time histogram of simultaneous inversion results from total 117,801 of P and S-P phase

constraints on focal depth parameters, as suggested by previous studies (**Gomberg et al., 1990**; **Husen & Hardebeck, 2010**). Given the close interrelation between the resolution test and seismic tomography inversion, the subsequent subchapter presents the seismic tomography results obtained from the horizontal and vertical cross-sectional views. They provided a comprehensive interpretation of the tectonic conditions in the research area.

3.1. Resolution Tests

The effectiveness of synthetic model inversion, validated by the input tests shown in **Figure 6a** and **Figure 6d**, is prominently depicted in **Figure 6b, Figure 6c, Figure 6e,** and **Figure 6f**, specifically for depths within the range of 20 to 50 km in the vicinity of Sumatra Island. This notable performance enabled the reliable interpretation of inversion outcomes at these particular depth intervals. The results of the CRT performance at a depth of 80-150 km and other depths shallower than 80 km can still be interpreted within the context of the geological structure within that depth range, as illustrated in Supplementary Material **Figure S2**. The performance was closely related to the different stations and earthquake distributions in each area of Sumatra Island. The oblique cross-section from A-A' to I-I' (which did not align with the west-east or north-south directions) did not result in a clear positive-negative anomaly pattern between the grids in the horizontal axis of the vertical sections. Instead, the positive-negative anomaly pattern was only observable in the vertical axis below the grids (see **Figure 7**). Besides conducting CRT tests, synthetic tests with a single negative anomaly block were also performed in this study, measuring 400 x 400 km². The test results also demonstrate satisfactory results up to a depth of 150 km, as shown in Supplementary **Figure S3**.

3.2. Vp Models

The number of tomograms expressed in terms of the P– wave velocity perturbation value or relative to the initial model was used as the inversion tomography input. This value shows the geological structure or tectonic conditions in the research area, represented by a negative anomaly (red) or a positive anomaly (blue). The positive anomaly observed in the seismic tomography results can be attributed to the subsurface structure, which exhibits a higher velocity compared to the initial model. This anomaly is associated with a high-density structure, resulting in faster wave propagation within the medium. Subduction slabs are notable examples of positive anomalies in seismic tomography studies (**Liu et al., 2019**; **Supendi et al., 2020**). In contrast to the positive anomaly, a negative anomaly was observed, indicating its association with prominent geological features, including faults, partial melting zones, magma reservoirs, fluid-rich zones, and elevated temperatures.
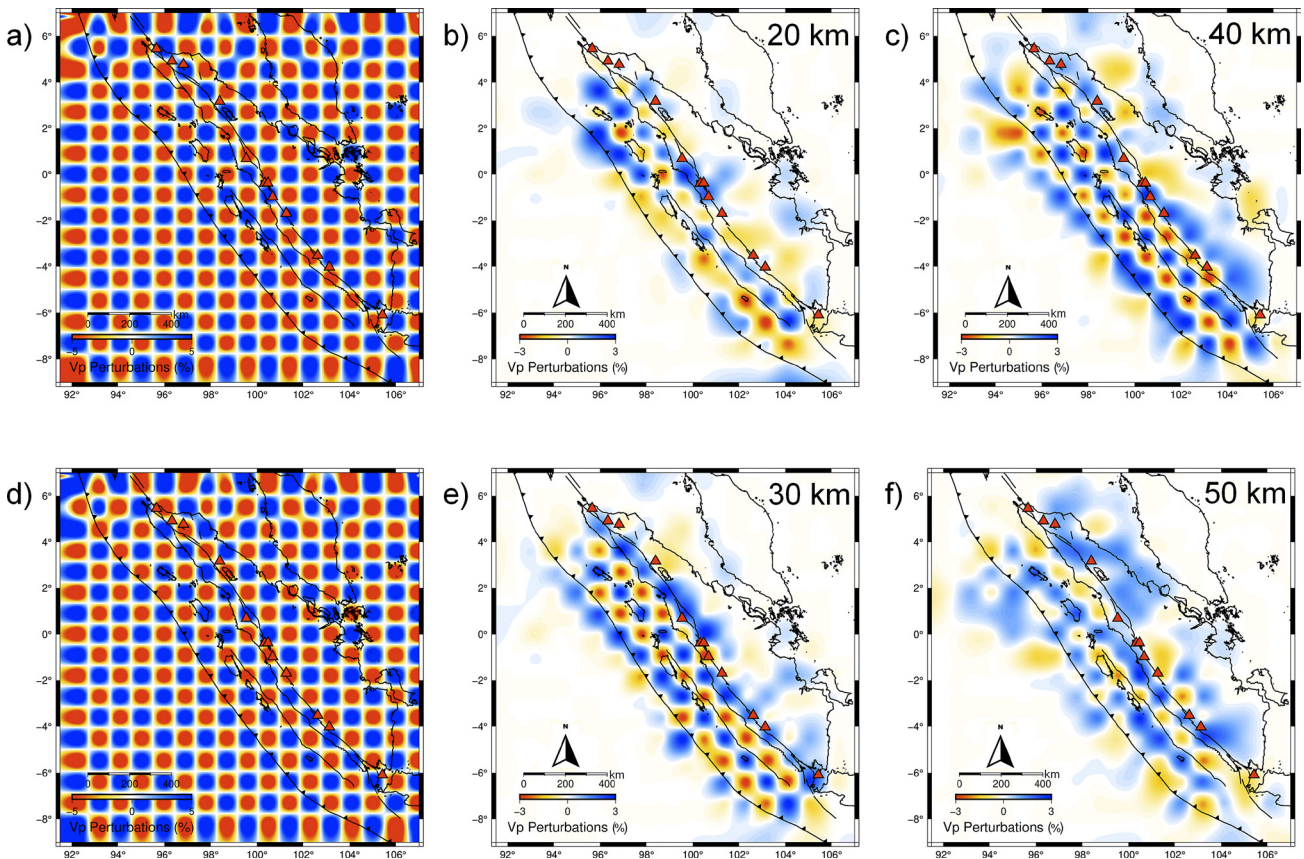
Figure 6: Checkerboard resolution test (CRT) Vp results for horizontal sections at a depth of 20, 30, 40, 50 km.
The CRT velocity model input for the top (a) corresponds to tomograms at depths of 20 km (b) and 40 km (c),
while the CRT velocity model input for the bottom (d) corresponds to tomograms at depths of 30 km (e) and 50 km (f).
Positive and negative perturbations of ±5% for input velocity model of CRT relative to the 1-D reference velocity model.
The velocity shown is relative to the AK135 1D model (**Kennett et al., 1995**).

The horizontal section shown in **Figure 8** and Supplementary **Figure S4** shows a positive anomaly extending along Sumatra from 0 to 150 km depth, which was indicated as a subduction slab of the Indo-Australian Plate subducting under the Eurasian Plate. The positive anomaly also moved northeast with increasing depth. A dominant negative anomaly is observed in the horizontal section at depths shallower than 30 km. This anomaly was most likely associated with a series of volcanoes on the island of Sumatra, known as the volcanic front line. Apart from being caused by a volcanic arc, this anomaly may also be related to the Sumatran Fault because the two positions are close. In order to achieve a more comprehensive understanding of the tectonic framework surrounding Sumatra Island, this study provides a series of nine vertical sections spanning from the northern to the southern regions of Sumatra. These sections are visualized in **Figure 9**, **Figure 10**, and **Figure 11**, enhancing the clarity of the tectonic picture.

The vertical tomogram from A–A' to I–I' shows that the depth of the subduction slab becomes deeper towards the south. This feature was related to the age of the slab, which increased in this direction (**Scotese et al., 1988**). This age relationship can be seen from the distribution of earthquakes that occurred north of Sumatra at a depth of

less than 180 km (see Figure 2), where the subduction slab plunged more and more to the south.

3.3. Northern Sumatra Tomographic Profiles (Section A to Section C)

The transverse lines A–A' in **Figure 9a** are cross-sections that intersect the Sunda Trench, Kota Aceh, and Sumatran Faults in the Seulimeum and Aceh segments, as shown in **Figure 1**. Positive anomalies represented in blue begin to appear from a depth of 30 km in the forearc area to less than 150 km beneath the Sumatra Island arc, considered a part of the Indo-Australian subduction slab in the province of Aceh. This positive anomaly was in line with the distribution of the earthquake hypocentre at medium depth, which resembles the Benioff Zone. A sizeable negative anomaly with dense earthquake distribution at 0–20 km depth on the right was most likely associated with the Sumatran Fault Zone in the Seulimeum and Aceh segments and the 2018 Pidie Jaya earthquake zone. Owing to the proximity of the volcanic arc and the Sumatran Fault, this strong negative anomaly might also have been caused by the magma system under the Seulawah Agam Volcano. The limited resolution of seismic data causes two anomalies generated by the Sumatran Fault, and the volcanic arc could not be sepa-
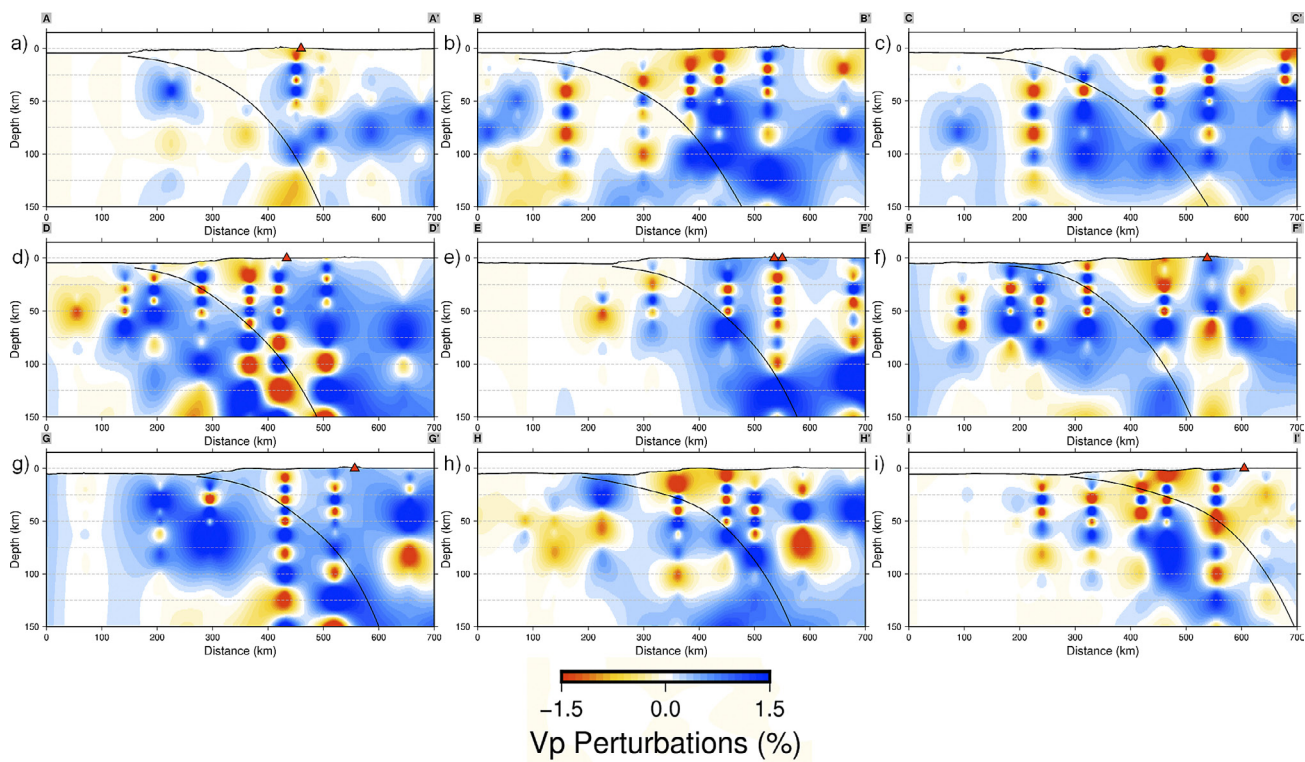
Figure 7: Checkerboard resolution test (CRT) Vp results for vertical sections in the cross-section direction A–A' to I–I' (a-i). The direction of the oblique/diagonal cross-section intersects the grid, displaying a CRT pattern that is not as distinct as the CRT results from a horizontal cross-section. To visualize anomaly patterns more clearly, the color perturbation scale is set to ± 1.5%.
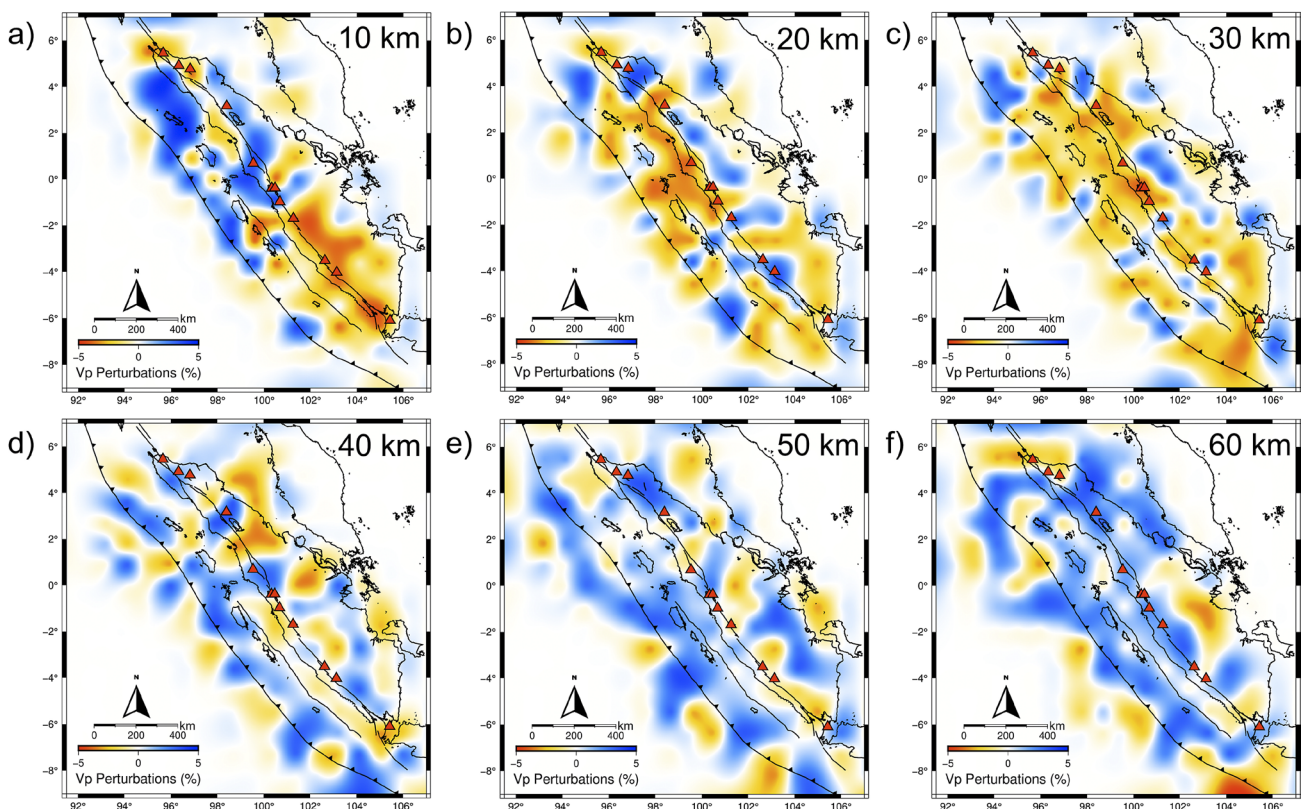
Figure 8: *Vp* tomogram for a horizontal section at 10 km (a), 20 km (b), 30 km (c), 40 km (d), 50 km (e), and 60 km (f) depth.

rated too clearly. In this cross-section, a partial melting zone was identified at a depth exceeding 100 km, exhibiting a negative anomaly that extended vertically to the base of the Seulawah Agam Volcano. This zone served as the magma source for the underlying magma reservoir. The 2018 Pidie Jaya earthquake (Event 14) occurred between moderate and robust negative anomalies in the contact zone. Negative anomalies are commonly observed beneath fault zones and are associated with stress concentrations, making these areas prone to earthquakes (**Nugraha et al., 2013**). The negative anomaly above the subduction slab in the southern part of the Seulawah Agam Volcano was likely linked to a mantle wedge structure. Similar negative anomalies were also identified above the subduction zone, specifically southwest of Toba Volcano, indicating the influence of the IFZ subduction (**Koulakov et al., 2016**).

Not much different from the A–A' cross-section, positive anomaly imaged in the B–B' and C–C' cross-sections (see **Figure 9b** and **Figure 9c**) and the earthquake hypocentre distribution in the Benioff Zone confirmed the presence of the Indo-Australian Plate subduction slab below the Eurasian Plate. The negative anomaly with a dense earthquake distribution at 0–20 km depth on the left side of these images was probably associated with the West Andaman Fault Zone through which the cross-section passes (**Martin et al., 2014**).

In the B-B' section, the 2010 Aceh earthquake (event 6) with a magnitude of 7.8 (**Ekström et al., 2012**) occurred, featuring a hypocentre at a lesser depth than the 2004 great earthquake (event 1). However, when examining the 2004 Aceh-Andaman earthquake segment, it becomes apparent that the 2010 Aceh earthquake occurred within that very same segment (**Ammon et al., 2005**). Although it caused strong level-V shocks on the MMI scale, the 2010 Aceh earthquake did not produce a tsunami (**Reliefweb, 2010**). The most plausible explanation is that the segment had already entered an inter-seismic state, where the stress accumulation had been released when the Aceh-Andaman 2004 earthquake.. The event emerged from shallower crust destabilization in response to a previously large earthquake. These factors make the submarine deformation energy insignificant to generate a tsunami. This event also indicated that the segment was resetting its recurrence at large earthquake intervals.

The 2004 Aceh-Andaman earthquake (event 1) and the 2005 Nias earthquake (event 2) occurred in the Indo-Australian Plate interface zone that subducts to the Eurasian Plate, as shown in **Figure 9c**. The rupture zone or segment of the two earthquakes was side-by-side (**Ammon et al., 2005**). Events 1 and 2 have the same perturbation characteristics, as indicated by the high *Vp* perturbation (see **Figure 9c**). This slight difference means the event 1 Aceh-Andaman earthquake rupture did not propagate towards Nias Island because it was below the southern boundary of the rupture zone where there were fold slabs in the upper and lower mantle transition zones,
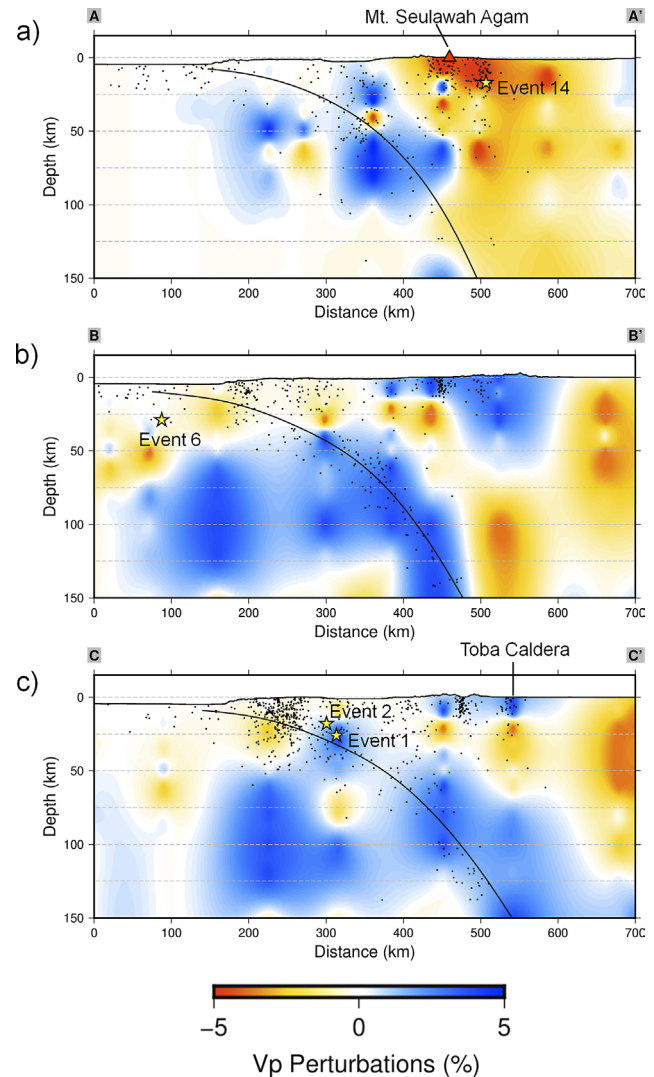
Figure 9: *Vp* tomographic inversion results for vertical sections A–A' (a), B–B' (b), and C–C' (c). The positions of the earthquake hypocentre (small black circle), the volcano (red triangle), and significant earthquakes (yellow star) are all located within a distance of 50 km from the vertical cross-section line. The black line on the vertical tomogram cross-section indicates the Slab 2.0 model (**Hayes et al., 2018**).

indicating the megathrust segmentation in the island (**Pesicek et al., 2008**). Based on **Figure 9c**, this section also passed through the northern part of the Toba Caldera, which had a negative perturbation anomaly at 25-50 km depth associated with the basic magma reservoir (**Koulakov et al., 2016**).

3.4. Central to Southern Sumatra Tomography Profiles (Section D to Section I)

The vertical section D–D' in **Figure 10a** is a cross-section that crosses Nias Island and the Sumatran Fault in the Toru, Angkola, and Barumun segments. The vertical section shows the accretionary prism complex on Nias Island and the Sumatran Fault Zone at a depth of less than 20 km.
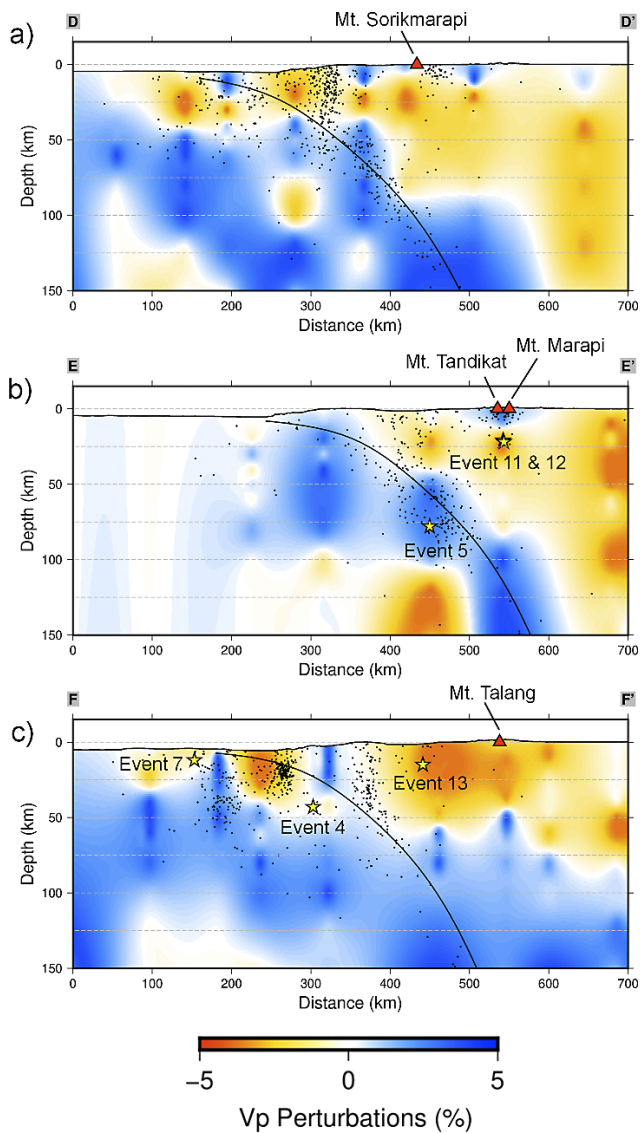
Figure 10: *Vp* tomographic inversion results for vertical sections D–D' (a), E–E' (b), and F–F'(c). The positions of the earthquake hypocentre (small black circle), the volcano (red triangle), and significant earthquakes (yellow star) are all located within a distance of 50 km from the vertical cross-section line. The black line on the vertical tomogram cross-section indicates the Slab 2.0 model (**Hayes et al., 2018**).

Figure 11: *Vp* tomographic inversion results for vertical sections G–G' (a), H–H' (b), and I–I'(c). The positions of the earthquake hypocentre (small black circle), the volcano (red triangle), and significant earthquakes (yellow star) are all located within a distance of 50 km from the vertical cross-section line. The black line on the vertical tomogram cross-section indicates the Slab 2.0 model (**Hayes et al., 2018**).

This region was associated with negative anomalies and high seismicity. **Barber et al., (2005)** described a diagram of the Sumatran subduction system showing Nias Island as part of an accretionary prism zone. The accretionary prism zone is characterized by the accumulation of uplifted sediments to produce new small islands. This vertical section also showed a partial melting zone, indicated by a negative anomaly as magma feeding for the Sorikmarapi Volcano. The positive anomaly was associated with the slab widening to the east (deflected) at a depth of 150 km. The anomaly extends away from the Benioff Zone curve and was represented by the earthquake hypocentre. The same phenomenon was also observed in the cross-section of E–E',

as shown in **Figure 10b**. As indicated by the CRT test, the CRT resulted in the slab area were valid, as shown in Supplementary **Figure S2e**. However, further S–wave tomography studies and other geophysical methods were required to confirm this hypothesis. The 2009 Padang earthquake (event 5) occurred in the intraslab zone and was associated with positive anomalies, as seen in sections E–E'. The earthquake was one of the largest intraslab earthquakes ever recorded on the island of Sumatra after 2000 (**Ekström et al., 2012**). Doublet earthquakes (events 11 and 12) were observed on the cross-section associated with a negative anomaly.

The vertical cross-section F–F' shown in **Figure 10c** was a cross-section that cut through the Sunda Trench,
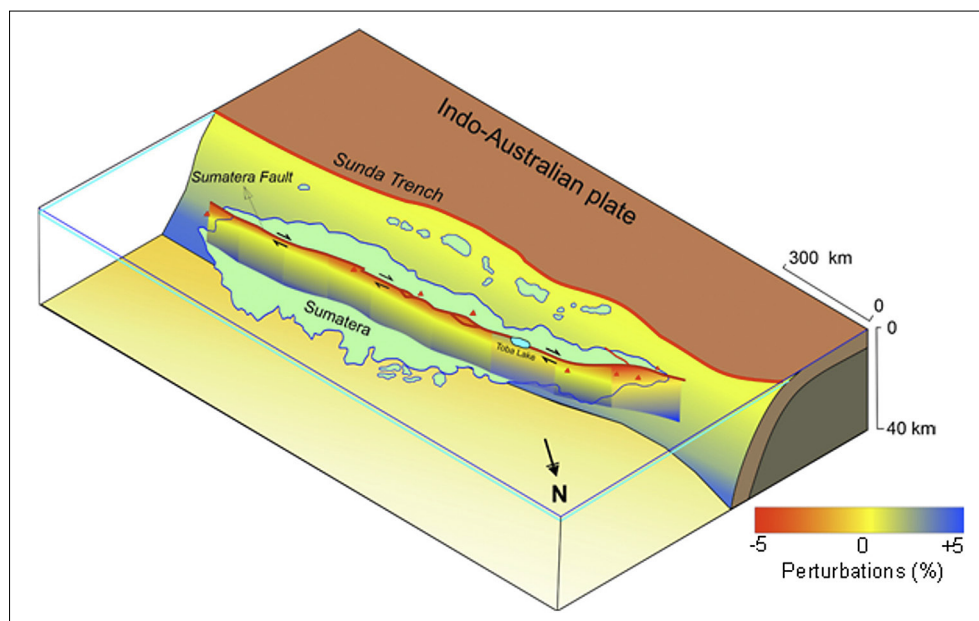
Figure 12: The tectonic framework of Sumatra Island and its adjacent areas discerned from the analysis of nine vertical cross-sections of P-wave tomography

Mentawai Fault, and Sumatran Fault in the Dikit segment, in which one of the significant earthquakes in the Sumatran Fault occurred (event 13). The cross-sectional tomogram in this section showed anomalous variations at a depth of 0–40 km, a dense collection of earthquakes occupying the negative anomaly area, which was an accretionary prism complex and weak zone in the Mentawai and Sumatran Faults in the Dikit segment. Two significant earthquake events, namely, the 2007 Bengkulu aftershock (event 4) and the 2010 Mentawai earthquake (event 7), occurred within the zone associated with the positive anomaly. Earthquakes within the oceanic slab commonly manifest as positive anomalies or regions with high *Vp* values attributed to the high density of the slab. This phenomenon was evident in the 2018 Lombok earthquake series, consisting of an event of Mw 6.4 event on July 29, 2018, and an Mw 7.0 event on August 5, 2018. Both earthquakes occurred within the Flores Oceanic Crust, which exhibited a notably high *Vp* anomaly (**Afif et al., 2021**).

The vertical cross-sections G–G' and H–H' in **Figure 11a** and **Figure 11b** intersected the Sunda Trench, Mentawai Fault, and Sumatran Fault in the Ketaun and Musi segments. The slab slope of the two vertical sections was sharper than that of the northern section owing to the age of the slab, which was aging in the south direction (**Scotese et al., 1988**). The 2007 Bengkulu earthquake (event 3) occurred in the interface zone, represented in vertical section G–G'. Rupture modelling based on GPS data showed a large slip under the archipelagic belt and shallow waters; therefore, the earthquake did not cause a significant tsunami (**Ambikapathy et al., 2010**). The cross-sectional tomogram in this section showed a positive anomaly aligned with the subduction slab, represented by an earthquake in the Benioff Zone. The slab model on the G–G' transverse line appeared to be a negative

anomaly under the forearc. This negative anomaly was thought to be related to slab dehydration. Subduction slabs and oceanic crust carried away large amounts of seawater in the pores and hydro minerals. As a result of the increase in temperature and pressure caused dehydration (release of water content) towards the crust layer above it. At shallow depths, water was expelled by subducting sediment compaction and loss of porosity in the upper oceanic crust. At a depth of approximately 100 km, this fluid could cause a partial melting phenomenon that causes the formation of a volcanic arc (**Tatsumi, 1989**). Most of the fluid is released under the forearc, and some is released under the back-arc. The presence of these hydro minerals caused a decrease in seismic velocity such that the anomaly value becomes negative (**Hyndman & Peacock, 2003**). The transverse line I–I' in **Figure 11c** is a vertical section that intersects the Sunda Trench, the Mentawai Fault, and the Mount Krakatau complex. In this section, the negative anomaly in the forearc section was related to slab dehydration and beneath the Mount Krakatau complex, which was related to the magma reservoir beneath the mountain complex. This negative anomaly could also be related to the Sumatran Fault in the Sunda segment through which this section passes.

The study findings allowed for the depiction of a tectonic model showing the geological features of Sumatra Island and its surrounding region, as depicted in **Figure 12**. The chromatic gradient from orange to red corresponds to low-velocity anomalies, whereas the gradient from green to blue signifies high-velocity anomalies. Low-velocity anomalies are associated with the volcanic arc and Sumatran Fault Zone, while high-velocity anomalies characterize the subduction zone, with deeper regions displaying increasing blue hues indicative of elevated velocity and density values within the slab.

4. Conclusions

The successful implementation of the simultaneous inversion method in this study has led to the development of a novel local-regional seismic tomography model for P-waves utilizing the BMKG seismic network. Comprehensive mapping of the slab geometry from northern to southern Sumatra revealed distinct patterns down to a depth of 150 km, with a notable increase in a slope towards the southern regions attributed to the influence of the older slab. Furthermore, the analysis has effectively captured key geological features, including the partial melting zone, mantle wedge structures, volcanic arcs, and Sumatran Fault Zone. The spatial correlation observed between significant earthquakes and their respective sources highlights the positive anomalies associated with subduction zone events and negative anomalies linked to earthquakes originating from the Sumatra Fault Zone. These findings emphasize the significant role of the BMKG seismic network in facilitating comprehensive local-regional seismic tomography studies and enabling the identification of previously undetected features. To further enhance the understanding, future studies should prioritize the repicking of the S-wave phase to obtain Vp/Vs tomograms, enabling a more accurate determination of the physical properties of the rocks.

Data availability

Raw data were generated at the Center for Earthquakes and Tsunami (PGT), BMKG. Derived data supporting the findings of this study are available from the corresponding author MR on request.

5. References

Papers:

Afif, H., Nugraha, A. D., Muzli, M., Widiyantoro, S., Zulfakriza, Z., Wei, S., Sahara, D. P., Riyanto, A., Greenfield, T., Puspito, N. T., Priyono, A., Sasmi, A. T., Supendi, P., Ardianto, A., Syahbana, D. K., Rosalia, S., Cipta, A., & Husni, Y. M. (2021). Local earthquake tomography of the source region of the 2018 Lombok earthquake sequence, Indonesia. *Geophysical Journal International, 226*(3), 1814–1823. https://doi.org/10.1093/gji/ggab189

Ambikapathy, A., Catherine, J., Gahalaut, V., Narsaiah, M., Bansal, A., & Mahesh, P. (2010). The 2007 Bengkulu earthquake, its rupture model and implications for seismic hazard. *Journal of Earth System Science, 119*(4), 553–560. https://doi.org/10.1007/s12040-010-0037-2

Ammon, C. J., Ji, C., Thio, H.-K., Robinson, D., Ni, S., Hjorleifsdottir, V., Kanamori, H., Lay, T., Das, S., Helmberger, D., & others. (2005). Rupture process of the 2004 Sumatra-Andaman earthquake. *Science, 308*(5725), 1133–1139. https://doi.org/10.1186/BF03353379

Barber, A. J., Crow, M. J., & Milsom, J. S. (2005). *Sumatra: Geology, Resources and Tectonic Evolution*. Geological Society of London. https://doi.org/10.1144/GSL.MEM.2005.031

DeMets, C., Gordon, R. G., & Argus, D. F. (2010). Geologically current plate motions. *Geophysical Journal International, 181*(1), 1–80. https://doi.org/10.1111/j.1365-246X.2009.04491.x

Earthquake Engineering Research Institute (EERI). (2009). Learning from earthquakes the Mw 7.6 Western Sumatra earthquake of September 30, 2009. *EERI Special Earthquake Report, 2009*, 1–12.

Ekström, G., Nettles, M., & Dziewoński, A. (2012). The global CMT project 2004–2010: Centroid-moment tensors for 13,017 earthquakes. *Physics of the Earth and Planetary Interiors, 200*, 1–9. https://doi.org/10.1016/j.pepi.2012.04.002

Fauzi, McCaffrey, R., Wark, D., Sunaryo, & Haryadi, P. Y. P. (1996). Lateral variation in slab orientation beneath Toba Caldera, northern Sumatra. *Geophysical Research Letters, 23*(5), 443–446. https://doi.org/10.1029/96GL00381

Fujii, Y., Satake, K., Watada, S., & Ho, T.-C. (2020). Slip distribution of the 2005 Nias earthquake (M w 8.6) inferred from geodetic and far-field tsunami data. *Geophysical Journal International, 223*(2), 1162–1171. https://doi.org/10.1093/gji/ggaa384

Gomberg, J. S., Shedlock, K. M., & Roecker, S. W. (1990). The effect of S-wave arrival times on the accuracy of hypocenter estimation. *Bulletin of the Seismological Society of America, 80*(6A), 1605–1628.

Haridhi, H. A., Huang, B.-S., Kuo-Liang, W., Denzema, D., Prasetyo, R. A., & Chao-Shing, L. (2018). A study of large earthquake sequences in the Sumatra subduction zone and its possible implications. *TAO: Terrestrial, Atmospheric and Oceanic Sciences, 29*(6), 6. https://doi.org/ 10.3319/TAO.2018.08.22.01

Hayes, G. P., Moore, G. L., Portner, D. E., Hearne, M., Flamme, H., Furtney, M., & Smoczyk, G. M. (2018). Slab2, a comprehensive subduction zone geometry model. *Science, 362*(6410), 58–61. https://doi.org/10.1126/science.aat4723

Husen, S., & Hardebeck, J. (2010). Earthquake location accuracy. *CORSSA*. https://doi.org/10.5078/corssa-55815573

Hyndman, R. D., & Peacock, S. M. (2003). Serpentinization of the forearc mantle. *Earth and Planetary Science Letters, 212*(3–4), 417–432. https://doi.org/10.1016/S0012-821X(03)00263-2

Kennett, B. L. N., Engdahl, E. R., & Buland, R. (1995). Constraints on seismic velocities in the Earth from traveltimes. *Geophysical Journal International*, *122*(1), 108–124. https://doi.org/10.1111/j.1365-246X.1995.tb03540.x

Koulakov, I., Kasatkina, E., Shapiro, N. M., Jaupart, C., Vasilevsky, A., El Khrepy, S., Al-Arifi, N., & Smirnov, S. (2016). The feeder system of the Toba supervolcano from the slab to the shallow reservoir. *Nature Communications*, *7*(1), 1–12. https://doi.org/10.1038/ncomms12228

Koulakov, I., Yudistira, T., & Luehr, B.-G. (2009). P, S velocity and VP/VS ratio beneath the Toba caldera complex (Northern Sumatra) from local earthquake tomography. *Geophysical Journal International*, *177*(3), 1121–1139. https://doi.org/10.1111/j.1365-246X.2009.04114.x

Lévêque, J.-J., Rivera, L., & Wittlinger, G. (1993). On the use of the checker-board test to assess the resolution of tomographic inversions. *Geophysical Journal International*, *115*(1), 313–318. https://doi.org/10.1111/j.1365-246X.1993.tb05605.x

Liu, S., Suardi, I., Yang, D., Wei, S., & Tong, P. (2018). Teleseismic traveltime tomography of northern Sumatra. *Geophysical Research Letters*, *45*(24), 13–231. https://doi.org/10.1029/2018GL078610

Liu, S., Suardi, I., Zheng, M., Yang, D., Huang, X., & Tong, P. (2019). Slab morphology beneath northern Sumatra revealed by regional and teleseismic traveltime tomography. *Journal of Geophysical Research: Solid Earth*, *124*(10), 10544–10564. https://doi.org/10.1029/2019JB017625

Malawani, M. N., Lavigne, F., Gomez, C., Mutaqin, B. W., & Hadmoko, D. S. (2021). Review of Local and Global Impacts of Volcanic Eruptions and Disaster Management Practices: The Indonesian Example. *Geosciences*, *11*(3), Article 3. https://doi.org/10.3390/geosciences11030109

Martin, K. M., Gulick, S. P. S., Austin Jr., J. A., Berglar, K., Franke, D., & Udrekh. (2014). The West Andaman Fault: A complex strain-partitioning boundary at the seaward edge of the Aceh Basin, offshore Sumatra. *Tectonics*, *33*(5), 786–806. https://doi.org/10.1002/2013TC003475

Masturyono, McCaffrey, R., Wark, D. A., Roecker, S. W., Fauzi, Ibrahim, G., & Sukhyar. (2001). Distribution of magma beneath the Toba caldera complex, north Sumatra, Indonesia, constrained by three-dimensional P wave velocities, seismicity, and gravity data. *Geochemistry, Geophysics, Geosystems*, *2*(4). https://doi.org/10.1029/2000GC000096

Meltzner, A. J., Sieh, K., Abrams, M., Agnew, D. C., Hudnut, K. W., Avouac, J., & Natawidjaja, D. H. (2006). Uplift and subsidence associated with the great Aceh-Andaman earthquake of 2004. *Journal of Geophysical Research: Solid Earth*, *111*(B2). https://doi.org/10.1029/2005JB003891

Mukti, M. M., Maulin, H. B., & Permana, H. (2021). Growth of forearc highs and basins in the oblique Sumatra subduction system. *Petroleum Exploration and Development*, *48*(3), 683–692. https://doi.org/10.1016/S1876-3804(21)60054-X

Muzli, M., Umar, M., Nugraha, A. D., Bradley, K. E., Widiyantoro, S., Erbas, K., Jousset, P., Rohadi, S., Nurdin, I., & Wei, S. (2018). The 2016 Mw 6.5 Pidie Jaya, Aceh, North Sumatra, earthquake: Reactivation of an unidentified sinistral fault in a region of distributed deformation. *Seismological Research Letters*, *89*(5), 1761–1772. https://doi.org/10.1785/0220180068

Nakano, M., Kumagai, H., Toda, S., Ando, R., Yamashina, T., Inoue, H., & Sunarjo. (2010). Source model of an earthquake doublet that occurred in a pull-apart basin along the Sumatran fault, Indonesia. *Geophysical Journal International*, *181*(1), 141–153. https://10.1111/j.1365-246X.2010.04511.x

Natawidjaja, D. H. (2018). *Updating active fault maps and sliprates along the Sumatran Fault Zone, Indonesia. 118*(1), 012001. https://doi.org/10.1088/1755-1315/118/1/012001

Nugraha, A. D., Ohmi, S., Mori, J., & Shibutani, T. (2013). High resolution seismic velocity structure around the Yamasaki fault zone of southwest Japan as revealed from travel-time tomography. *Earth, Planets and Space*, *65*(8), 871–881. https://doi.org/10.5047/eps.2012.12.004

Osagie, A. U., & Ahmad Abir, I. (2021). Seismic tomographic imaging of P wave velocity perturbation beneath Sumatra, Java, Malacca Strait, Peninsular Malaysia and Singapore. *Journal of Earth System Science*, *130*(1), 1–13. https://doi.org/10.1007/s12040-020-01530-w

Pesicek, J. D., Thurber, C. H., Widiyantoro, S., Engdahl, E. R., & DeShon, H. R. (2008). Complex slab subduction beneath northern Sumatra. *Geophysical Research Letters*, *35*(20). https://doi.org/10.1029/2008GL035262

Ramdhan, M., Widiyantoro, S., Nugraha, A. D., Métaxian, J.-P., Rawlinson, N., Saepuloh, A., Kristyawan, S., Sembiring, A. S., Budi-Santoso, A., Laurin, A., & Fahmi, A. A. (2019). Detailed seismic imaging of Merapi volcano, Indonesia, from local earthquake travel-time tomography. *Journal of Asian Earth Sciences*, *177*, 134–145. https://doi.org/10.1016/j.jseaes.2019.03.018

Rawlinson, N., & Spakman, W. (2016). On the use of sensitivity tests in seismic tomography. *Geophysical Journal International*, *205*(2), 1221–1243. https://doi.org/10.1093/gji/ggw084

Scotese, C. R., Gahagan, L. M., & Larson, R. L. (1988). Plate tectonic reconstructions of the Cretaceous and Cenozoic ocean basins. *Tectonophysics*, *155*(1–4), 27–48. http://doi.org/10.1016/0040-1951(88)90259-4

Sieh, K., & Natawidjaja, D. (2000). Neotectonics of the Sumatran fault, Indonesia. *Journal of Geophysical Research: Solid Earth*, *105*(B12), 28295–28326. https://doi.org/10.1029/2000JB900120

Supendi, P., Nugraha, A. D., Widiyantoro, S., Abdullah, C. I., Rawlinson, N., Cummins, P. R., Harris, C. W., Roosmawati, N., & Miller, M. S. (2020). Fate of Forearc Lithosphere at Arc-Continent Collision Zones: Evidence From Local Earthquake Tomography of the Sunda-Banda Arc Transition, Indonesia. *Geophysical Research Letters*, *47*(6), e2019GL086472. https://doi.org/10.1029/2019GL086472

Tatsumi, Y. (1989). Migration of fluid phases and genesis of basalt magmas in subduction zones. *Journal of Geophysical Research: Solid Earth*, *94*(B4), 4697–4707. https://doi.org/10.1029/JB094iB04p04697

Um, J., & Thurber, C. (1987). A fast algorithm for two-point seismic ray tracing. *Bulletin of the Seismological Society of America, 77*(3), 972–986. https://doi.org/10.1785/BSSA 0770030972

Wadati, K. (1933). On the travel time of earthquake waves (Part I). *Geophys. Mag., 7*, 87–99. https://cir.nii.ac.jp/crid /1571417124417426560

Weatherall, P., Marks, K. M., Jakobsson, M., Schmitt, T., Tani, S., Arndt, J. E., Rovere, M., Chayes, D., Ferrini, V., & Wigley, R. (2015). A new digital bathymetric model of the world's oceans. *Earth and Space Science, 2*(8), 331–345. https://doi.org/10.1002/2015EA000107

Wessel, P., & Smith, W. H. (1998). New, improved version of Generic Mapping Tools released. Eos, Transactions American Geophysical Union, 79(47), 579-579. http://doi.org /10.1029/98EO00426

Widiyantoro, S., & van der Hilst, R. (1996). Structure and evolution of lithospheric slab beneath the Sunda arc, Indonesia. *Science, 271*(5255), 1566. https://doi.org/10.1126/science.271.5255.1566

Widiyantoro, S., & van der Hilst, R. (1997). Mantle structure beneath Indonesia inferred from high-resolution tomographic imaging. *Geophysical Journal International, 130*(1), 167–182. https://doi.org/10.1111/j.1365-246X. 1997.tb00996.x

Chapter in book:

Thurber, C. H. (1993). Local earthquake tomography: Velocities and Vp/Vs-theory. In H. M. Iyer & K. Hirahara (Eds.), Seismic Tomography: Theory and practice (pp. 563--583). Chapman and Hall.

Books:

Evans, J. R., Eberhart-Phillips, D., & Thurber, C. H. (1994). *User's manual for SIMULPS12 for imaging vp and vp/vs; a derivative of the 'Thurber' tomographic inversion SIMUL3 for local earthquakes and explosions* (Report No. 94–431; Open-File Report). USGS Publications Warehouse. https://doi.org/10.3133/ofr94431

Grandis, H. (2009). Pengantar pemodelan inversi geofisika. *Himpunan Ahli Geofisika Indonesia (HAGI)* (in *Indonesian*)

Irsyam, M., Widiyantoro, S., Natawidjaja, D., Meilano, I., Rudyanto, A., Hidayati, S., Triyoso, W., Hanifa, N., Djarwadi, D., Faizal, L., & others. (2017). Peta sumber dan bahaya gempa Indonesia tahun 2017. *Pusat Penelitian Dan Pengembangan Perumahan Dan Permukiman, Kementerian Pekerjaan Umum Dan Perumahan Rakyat (in Indonesian)*.

Ramdhan, M., Priyobudi, P., Imananta, R. T., Muzli, M., Supendi, P., Yusuf Hadi Perdana, Nugraha, J., Jatnika, J., Ali, Y. H., Panjaitan, A. L., Nugraha, M. F., Kristyawan, S., Sembiring, A. S., Setyahagi, A. R., & Yogaswara, D. S. (2021). *Katalog Gempabumi Indonesia: Relokasi Hiposenter dan Implikasi Tektonik* (1st ed., Vol. 1). Bidang Informasi Gempabumi dan Peringatan Dini Tsunami (BMKG) (in *Indonesian*)

Internet source:

Reliefweb. (2010, April 20). *M7.8 Northern Sumatra, Indonesia, Earthquake of 6 April 2010—Indonesia | ReliefWeb.* Reliefweb. URL: https://reliefweb.int/map/indonesia/ m78-northern-sumatra-indonesia-earthquake-6-april-2010 (accessed: 1st April 2023)

SAŽETAK

Seizmičko modeliranje na području otoka Sumatre i njegove okolice, Indonezija, pomoću P-valne seizmičke tomografije lokalnih i regionalnih potresa

Otok Sumatra i njegova okolica, Indonezija, jedno su od najaktivnijih tektonskih područja na svijetu. Tamo se dogodio potres Aceh-Andaman, jedan od najrazornijih potresa na svijetu. Privukao je mnoge znanstvenike koji su u svojim istraživanjima primijenili različite metode, uključujući seizmičku tomografiju, kako bi razumjeli podzemnu strukturu i tektonski sustav otoka. Ova studija prva je koja prikazuje model podzemlja ispod otoka i njegove okolice koristeći se lokalno-regionalnim katalogom potresa iz seizmičke mreže Indonezijske agencije za meteorologiju, klimatologiju i geofiziku (BMKG). Tomografski model brzine P-valova (Vp), uspješno je razgraničio subduciranu ploču (velika brzina P-valova), zonu djelomičnoga taljenja (mali Vp), vulkanski luk (mali Vp) i rasjedne zone Sumatre (mali Vp). Odnos između subdukcijske zone i vulkanskoga luka na otoku može se vidjeti na nekoliko vertikalnih presjeka gdje se na dubini od oko 100 km javlja zona djelomičnoga taljenja koja služi kao izvor magme za neke vulkane na otoku. Model oceanske subducirane ploče također pokazuje izraženiji i strmiji nagib prema južnim regijama otoka Sumatre, što se vjerojatno može pripisati procesu starenja ploče u tome smjeru. Rezultati naglašavaju važnost BMKG seizmičke mreže u identifikaciji lokalno-regionalnih podzemnih struktura ispod indonezijskoga arhipelaga, posebno za glavne otoke kao što je Sumatra.

Ključne riječi:
Sumatra, BMKG, P-val, tomografija, subducirana ploča, rasjed

Author's contribution

Bayu Pranata (1) (Dr.), **Mohamad Ramdhan (2)** (Dr.), **Muhammad Hanif (3)** (M.Sc) carried out tomography analyses, conceptualization, processing, and writing the manuscript. **Muhammad Iqbal Sulaiman (4)** (B.Sc) performed tomographic inversion. **Mufti Putra Maulana (5)** (B.Sc) conducted data visualization. **Wandono (6)** (Dr.), **Sri Widiyantoro (7)** (Prof. Dr.), **Sandy Kurniawan Suhardja (8)** (Dr.) & **Edi Hidayat (9)** (Dr.) contributed to the manuscript editing and interpretation of the results. **Pepen Supendi (10)** (Dr.) & **Ridwan Kusnandar (11)** (M.Sc) conducted data collection (resources). **Wiko Setyonegoro (12)** (M.Com) examined the results and manuscript editing.